Bull. Mater. Sci., Vol. 36, No. 4, August 2013, pp. 719–727. © Indian Academy of Sciences.

Effect of plating time on growth of nanocrystalline Ni–P from sulphate/glycine bath by electroless deposition method

N LATHA, V RAJ[†,*] and M SELVAM[††]

Department of Chemistry, Kandaswamy Kandar's College, Paramathy–Velur 638 182, India
[†]Advanced Materials Research Laboratory, Department of Chemistry, Periyar University, Salem 636 011, India
[††]Industrial Metal Finishing Division, Central Electrochemical Research Institute, Karaikudi 630 006, India

MS received 25 November 2011; revised 25 April 2012

Abstract. **Nanocrystalline nickel phosphorus (NC-Ni–P) deposits from sulphate/glycine bath using a simple electroless deposition process is demonstrated. In the present investigation, nanoporous alumina films are formed on the aluminium surface by anodization process followed by deposition of nickel onto the pores by electroless plating method. Anodic aluminium oxide surface was first sensitized and activated by using palladium chloride solution before immersing into the electroless nickel bath. Electroless nickel plating was carried out from the optimized bath by changing the deposition time from 20 to 1800 s at a constant temperature of 80 °C and a pH of 4·0. Surface morphology, elemental composition, structure and reflectance of the deposits have been analysed by using scanning electron microscopy, atomic force microscopy, energy dispersive X-ray analysis, X-ray diffractometry and UV-visible spectroscopic studies, respectively. Electroless nickel deposits formed at an early stage produces dense uniform nanocrystals containing higher percentage of atomic phosphorus with cubic Ni (111) structure. As the deposition time increased, nanocrystalline sharp peak became amorphous and dimension of the crystal size varied from 54 to 72 nm.**

Keywords. **NC-Ni–P; electroless deposition; aluminium; anodization.**

1. Introduction

Nanocrystalline nickel phosphorus (NC-Ni–P) deposition has been an emerging area for researchers and scientists due to its applications in chemical, aerospace, automobile and textile industries (Mallory and Hajdu 1990; Parker 1992), since the discovery of electroless nickel–phosphorus (ENP) coatings (Brenner and Riddell 1946) and nanoporous anodic alumina films (Masuda and Fukuda 1995). The high insulation ability of anodic oxide film formed on aluminium substrate is mainly of porous Al_2O_3 in the as formed condition. Metallization of these nanopores of AAO films will generate nanowires or nanorods.

Nanostructured metals have been prepared by various methods such as PVD, CVD, electrodeposition, electroless deposition, ball milling, mechanical alloying, severe plastic deformation, sol–gel techniques, etc (Chow and Ovid'ko 2000; Meyer *et al* 2006). Among these methods, electroless deposition is one of the most attractive methods for the formation of nanocrystalline structures (Shacham-Diamad and Sverdlov 2000). Ni–P can be prepared by electroless deposition (Sevugan *et al* 1993; Keong *et al* 2002) from solutions containing metal salt and sodium hypophosphite as a reducing agent.

In ENP coatings, variation in phosphorus content influences crystal structure and surface morphology of the deposit. ENP coatings containing 1·9–3·7 at.% P are crystalline/microcrystalline (Martyak and Drake 2000) and phosphorous content higher than 17·4 at.% are amorphous in nature (Kumar and Nair 1994). Alloys with intermediate compositions have semi-amorphous or amorphous structures (Apachitei *et al* 1998) and deposit with 20·3 at.% phosphorus content consists of nanocrystalline and not amorphous (Goldenstein *et al* 1957; Tyagi *et al* 1985; Hur *et al* 1990) structure. According to the literature, increase in phosphorus content decreases grain size of the as-deposited electroless Ni–P. Properties and growth of the coating are significantly affected by bath parameters such as electrolyte concentration, pH, temperature, deposition time and nature of substrates.

A complexing agent is required for the deposition of Ni–P; sodium acetate (Fundo and Abrantes 2007), citrate (Li *et al* 2005), lactate (Baskaran *et al* 2006) and glycine with acetate (Huang and Cui 2007) were studied as the complexing agents. The sulphate/glycine/sodium hypophosphite electrolyte can produce NC-Ni–P deposit of high structural quality. The present work deals with the effect of plating time on the morphology, crystalline structure and composition of NC-Ni–P coatings formed from the sulphate/glycine/sodium hypophosphite electrolyte by electroless plating method.

*Author for correspondence (alaguraj2@rediffmail.com)

2. Experimental

AA 1100 aluminium specimens with dimensions 7 × 1 × 0·1 cm were degreased in acetone, etched in a solution containing 50 g/l sodium hydroxide for 2 min at room temperature, rinsed well and immersed for 1 min in 20% (v/v) nitric acid at room temperature. All the solutions were prepared using double distilled water. The pretreated aluminium specimen was anodized in 10% sulphuric acid at a constant current density of 0·8 A/dm^2 at 20 ± 1 °C (with cooling and agitation) for 30 min to obtain porous anodic aluminium oxide film. Then the specimen was sensitized by immersing in a solution containing 10 g/l $SnCl_2$ and 40 ml/l HCl for 2 min at 30 °C and activated by dipping in a solution containing 1 g/l $PdCl_2$ and 10 ml/l HCl for 30 s at 30 °C. After each pretreatment step, the substrate was rinsed in deionized water. The entire procedure for the formation of Ni–P nanocrystals on aluminium surface is schematically represented in figure 1.

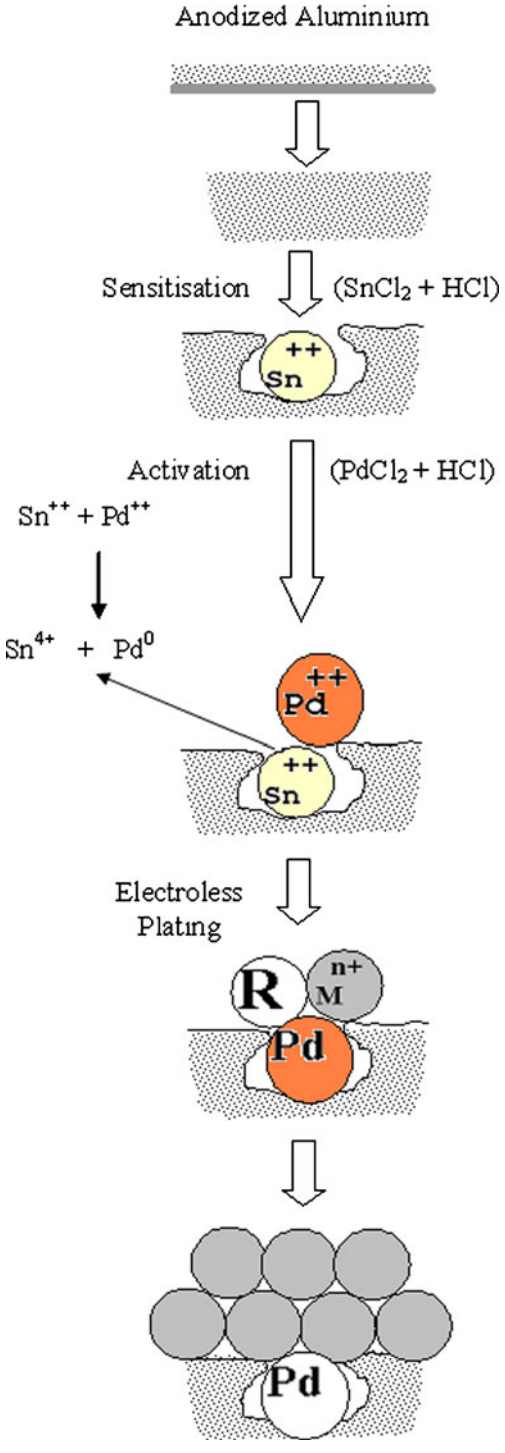

Figure 1. Schematic outline of electroless Ni–P plating on aluminium.

Electroless nickel (EN) plating was carried out immediately after activation. The optimized electroless Ni–P plating bath consisted of nickel sulphate (42 g/l), sodium hypophosphite (21 g/l), glycine (11 g/l) as the nickel ion provider, metal-reducing agent and complexing agent, respectively. Temperature of the bath was maintained at 80 °C. The pH of the plating bath was fixed at 4·0 and adjusted with 20% H_2SO_4 solution. EN bath is highly sensitive to impurities and hence prior to its use, the solution was filtered through Whatman No. 40 filter paper.

Morphological characterization of the coated specimens was carried out by scanning electron microscopy (SEM, JEOL-Japan-JSM-840A), atomic force microscopy (AFM) (Digital Instruments CP-II Veeco Company, USA) and the elemental composition of the deposits were analysed by energy dispersive X-ray spectroscopy (EDAX, Oxford link ISIS 300). The structure and grain size of the Ni–P deposits were determined using a Philips X'pert X-ray diffractometer (XRD) with CuKα radiation (λ = 0·15418 nm). UV-visible reflectance spectra of the electroless Ni–P deposit was recorded using Hitachi U-3400 spectrophotometer.

3. Results and discussion

3.1 *SEM analysis*

The surface morphology, crystalline growth and structure of NC-Ni–P deposits formed on anodized aluminium by electroless nickel plating were investigated by SEM analysis. SEM images of electroless Ni–P deposits on anodic aluminium oxide (AAO) film obtained at various deposition times from 20 to 1800 s are presented in figure 2(a–k). The Ni–P coatings formed at 20 and 30 s have nodular morphology as shown in figure 2(a, b). It indicates that, the honeycomb porous alumina layer of the film is completely covered by small crystals of Ni–P. The tiny Ni–P crystals formation on the AAO film is clearly observed at the deposition time of 50 s as shown in figure 2(c). Deposition of Ni–P coatings formed at 90 and 120 s under the same conditions, produced clusters of large number of homogeneous nanocrystalline black Ni–P. At this stage, nanocrystals are cojoined and coalesced to nucleation growth, which can be seen clearly in figure 2(d, e). By further increase in the deposition time from 180 to 1800 s, it can be observed that, the dimension

of the crystal size increases and the number of nanocrystals decreases as seen in figure 2(f–k) (Wang *et al* 2003). Dense coverage of Ni–P granular deposits is seen up to 300 s with crystals size in nanometer range and hence the Ni–P coatings are nanocrystalline in nature. When the deposition time is increased to 1800 s, spherical nodules are clearly observed in the coatings. It is supported by the earlier report (Lu and Zangari 2002). The deposit is compact and smooth throughout the coated surface in all deposition times without any cracks or defects. Variation in surface morphology of these coatings suggests a definite dependence on their phosphorus content (Zhao *et al* 2007). From the comparison of the surface morphologies, it can be found that, by increasing deposition time, moderate change in atomic percent of phosphorus in a parabolic fashion with increasing grain size of Ni–P alloy coatings is observed. It can also be found that, the grain size of Ni–P alloy coatings with phosphorus content above 20 at.% P indicates nanocrystalline structures. Energy dispersive spectroscopic analysis confirms phosphorus content in the electroless Ni–P coatings.

3.2 *EDAX analysis*

EDAX analysis was carried out to determine the composition of elements present in the coated specimen. Figure 3(a, b) shows EDAX spectra of the electroless Ni–P coatings on anodized aluminium at 30 and 1800 s, respectively. EN deposition process can be categorized into two steps. The first step is related to the formation of a thin film on the porous aluminium substrate and the second step is bulk coating. The mechanism of the first step consists of nucleation, growth and coalescence of crystals (Liu and Gao 2006).

In the first step of electroless nickel deposit at 30 s (figure 3(a)), the spectrum shows P, Ni and S peaks. The P peak in the EDAX spectrum reveals that phosphorus is co-precipitated with Ni during electroless nickel deposition. Presence of S peak may probably come from sulphuric acid anodizing bath (Goueffon *et al* 2009). Figure 3(b) is the EDAX spectrum of bulk deposit produced in 1800 s. The coating consists of only Ni and P elements and not sulphur element. EDAX spectrum clearly reveals that, increasing

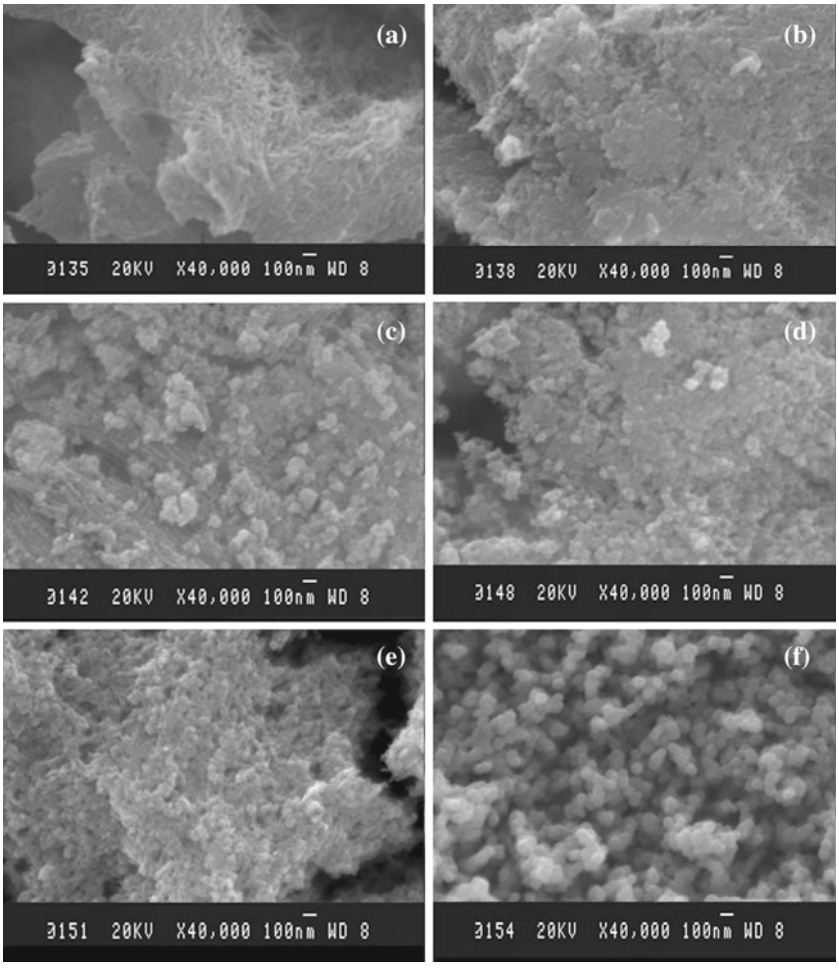

Figure 2. SEM images of electroless nickel deposits formed on anodized aluminium at various deposition times: (**a**) 20 s, (**b**) 30 s, (**c**) 50 s, (**d**) 90 s, (**e**) 120 s, (**f**) 180 s, (**g**) 300 s, (**h**) 600 s, (**i**) 900 s, (**j**) 1200 s and (**k**) 1800 s.

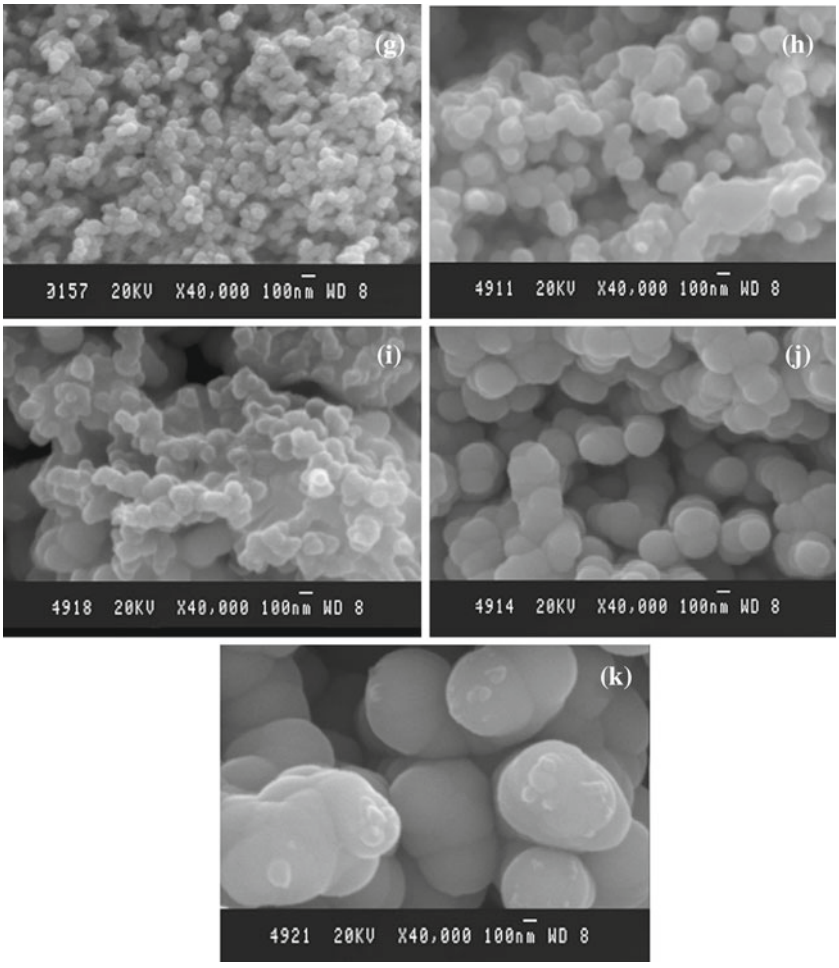

Figure 2. (*continued*).

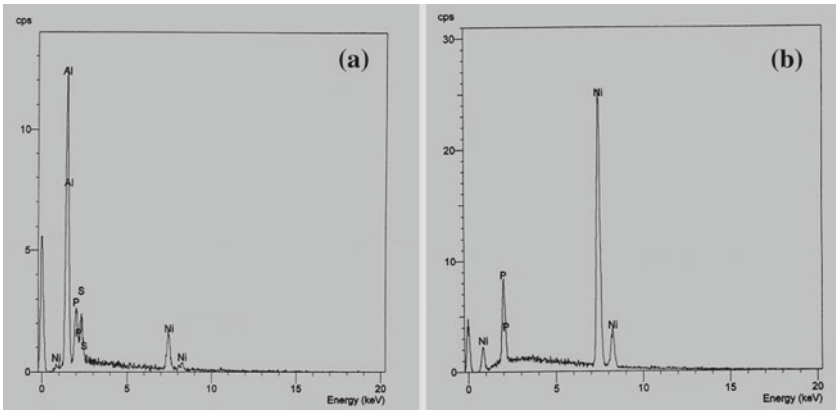

Figure 3. EDAX spectra of electroless Ni–P coatings formed on anodized aluminium: (**a**) 30 s and (**b**) 1800 s.

deposition time decreases the sulphur peak height and finally disappears. Correspondingly, the Ni peak height increases. It is revealed that the coating has higher content of phosphorus along with nickel and lesser amount of sulphur in the initial deposition time. As the deposition time increases, atomic percentage of phosphorus decreases. Similar trend has been reported earlier (Yajima *et al* 1987).

3.3 *AFM analysis*

Figures 4(a–c) and 5(a–c) show atomic force microscopic (AFM) images of (a) topographical image (2D), (b) three-dimensional (3D) image and (c) depth profile analysis of electroless nanocrystalline Ni–P deposits formed in 30 and 1800 s, respectively. It is clearly seen from figure 4(a, b)

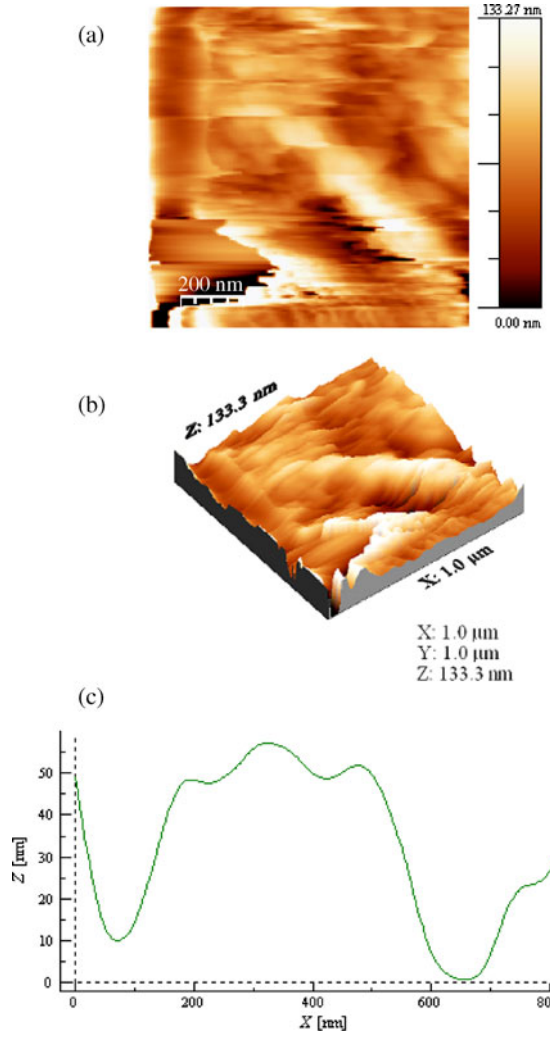

Figure 4. AFM images of as-deposited electroless Ni–P coating formed on anodized aluminium for deposition time of 30 s: (**a**) topographic image, (**b**) 3-dimensional image and (**c**) depth profile analysis.

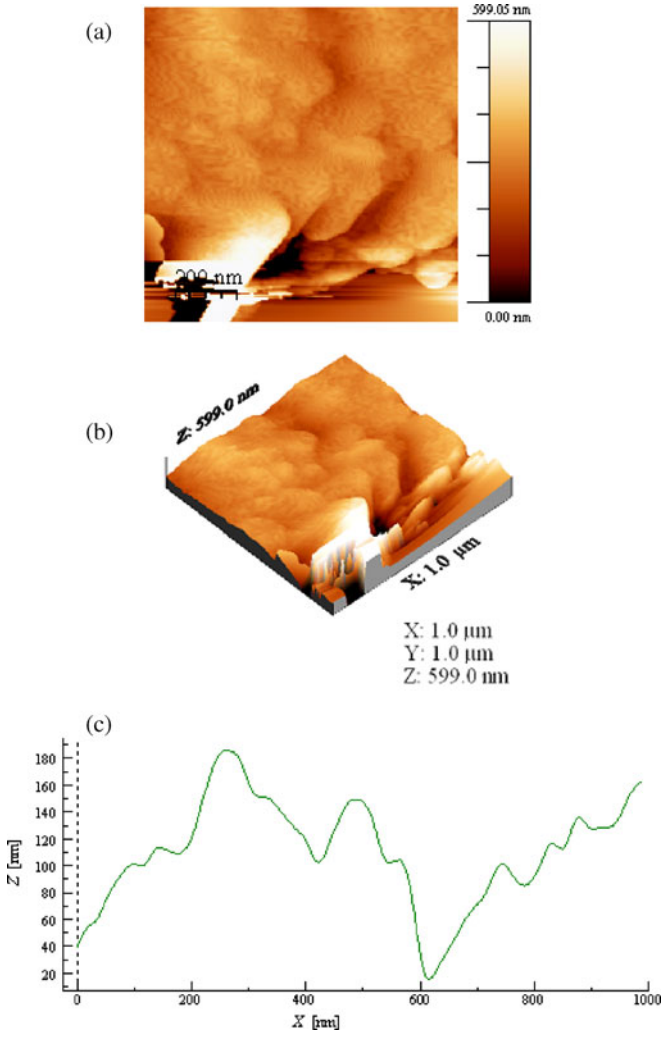

Figure 5. AFM images of as-deposited electroless Ni–P coating formed on anodized aluminium for deposition time of 1800 s: (**a**) topographic image, (**b**) 3-dimensional image and (**c**) depth profile analysis.

that electroless nickel coating formed in 30 s is composed of uniform layer of Ni–P nanocrystals. AAO surface was completely covered by black nanocrystals of Ni–P. There were no cracks or pits on the surface. Depth profile analysis in horizontal direction (figure 4(c)) shows small number of peaks in the measured surface area of 1×1 μm. Crystal size is in the range of 10–100 nm.

When electroless nickel deposition time is increased to 1800 s, coating has large number of Ni–P nanocrystals, combined to form almost uniform morphology as shown in figure 5(a, b). In this deposition time, no definite grains are found without any cracks. Figure 5(c) depicts depth profile analysis in the horizontal direction. Smaller peaks are present in the measured area of 1×1 μm. Crystal size is in the range of $<$100 nm. AFM results showed that surface of the coating is nanocrystalline and compact in the as-deposited state for both these deposition times.

Compared to that of anodized aluminium, average surface roughness (R_a) value is less for the as-deposited coating. It is due to filling of the nanopores by Ni–P on the AAO film during electroless Ni–P deposition process. Roughness value at 30 s is 58·2 nm and 1800 s is 36·3 nm and the corresponding root mean square (RMS) values are 79·7 and 46·5 nm, respectively. The roughness value reveals that electroless NC-Ni–P coating consists of a large number of nanocrystals in the nanoporous AAO film.

3.4 *XRD analysis*

X-ray diffraction patterns of the as-deposited samples formed at different deposition times from 20 to 1800 s are given in figure 6(a–k). The as-deposited coating contains nickel and phosphorus peaks. Average crystal size of the Ni–P coatings was calculated using Scherrer's equation,

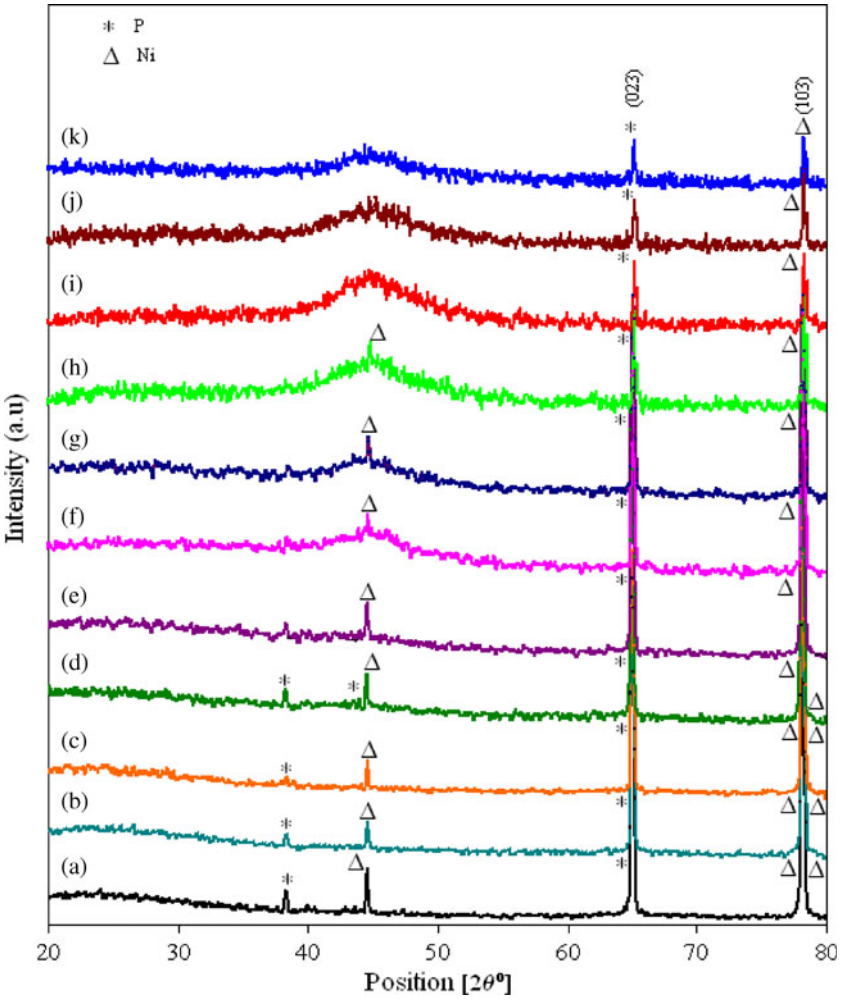

Figure 6. XRD patterns of electroless Ni–P coatings formed on anodized aluminium at various deposition times: (**a**) 20 s, (**b**) 30 s, (**c**) 50 s, (**d**) 90 s, (**e**) 120 s, (**f**) 180 s, (**g**) 300 s, (**h**) 600 s, (**i**) 900 s, (**j**) 1200 s and (**k**) 1800 s.

$D = 0{\cdot}9\ \lambda/\beta \cos\theta$ (Birks and Friedman 1946), where λ is the wavelength of radiation, β is the full width at half maximum (FWHM), θ is the diffraction angle of the main peak. Joint Committee of Powder Diffraction Standards (JCPDS) database card file index was used to analyse the XRD pattern. Peak positions (2θ), d-spacing values, plane orientations, structure and crystal size according to the JCPDS file are given in table 1.

Figure 6(a) shows XRD pattern of electroless Ni–P deposit formed at 20 s. It shows P (1 1 8) peak at 38·34° (JCPDS file no. 75-0577), Ni (0 1 1) peak at 44·58° (JCPDS file no. 45-1027), P (0 2 3) peak at 64·94° (JCPDS file no. 65-2491) and two Ni (1 0 3) peaks at 78·07° and 78·37° (JCPDS file no. 45-1027). For the deposition time of 30 s (figure 6(b)), XRD pattern of the coating shows two phosphorus peaks at 38·37° and 64·98° with (1 1 8) and (1 0 3) orientations, respectively and the Ni (1 1 1), (1 0 3) and (2 2 0) peaks at 44·61°, 78·11° and 78·41° (JCPDS file no. 01-1260, 45-1027, 88-2326), respectively. Figure 6(c) shows XRD pattern of electroless nickel deposit formed at 50 s. It gives the P (1 1 8) peak at 38·38° (JCPDS file no. 75-0577), Ni (1 1 1) peak at 44·61° (JCPDS file no. 01-1260), P (0 2 3) peak at 64·98° (JCPDS file no. 65-2491), Ni (1 0 3) peak at 78·11° (JCPDS file no. 45-1027) and Ni (2 2 0) peak at 78·40° (JCPDS file no. 88-2326). Figure 6(d) depicts XRD pattern of electroless nickel deposit formed at 90 s. It gives three phosphorus peaks at 38·27°, 43·55° and 64·91° corresponding to (1 1 8), (1 3 1) and (0 2 3) orientations, respectively and three nickel peaks at 44·53°, 78·04° and 78·33° corresponding to (1 1 1), (1 0 3) and (2 2 0) orientations, respectively. Figure 6(e) shows XRD pattern of electroless nickel deposit formed at 120 s. It gives four peaks at 38·23°, 44·58°, 64·94° and 78·08° corresponding to P (1 1 8), Ni (0 1 1), P (0 2 3) and Ni (1 0 3), respectively. Figure 6(f–h) shows electroless Ni–P deposit formed at 180, 300 and 600 s, respectively. The coating formed at 180 s gives three peaks at 44·53°, 65° and 78·13° and the coating formed at 300 s gives the same peaks at 44·70°, 65·03° and 78·16° and that formed at 600 s gives the same peaks at 44·93°, 65·15° and 78·28° corresponding to the same plane orientations Ni (1 1 1), P (0 2 3) and Ni (1 0 3), respectively.

Table 1. XRD results of electroless nanocrystalline Ni–P coatings formed on anodized aluminium at various deposition times.

Deposition time (s)	Position ($2\theta°$)	'*d*' observed	'*d*' standard	Indexing plane	JCPDS file no.	Lattice parameters a	b	c	Structure	Particle size (nm)	Average particle size (nm)
20	38·34	2·347	2·334	P(118)	75–0577	9·21	9·15	22·6	Monoclinic	42·75	54·34
	44·58	2·032	2·033	Ni(011)	45–1027	2·6515(4)		4·343(3)	Hexagonal	43·65	
	64·94	1·435	1·409	P(023)	65–2491	3·316	10·52	4·389	Orthorhombic	47·87	
	78·07	1·223	1·223	Ni(103)	45–1027	2·6515(4)		4·343(3)	Hexagonal	51·99	
	78·37	1·222	1·223	Ni(103)	45–1027	2·6515(4)		4·343(3)	Hexagonal	85·45	
30	38·37	2·345	2·3341	P(118)	75–0577	9·21	9·15	22·6	Monoclinic	28·50	48·31
	44·61	2·031	2·03	Ni(111)	01–1260	3·5175			Cubic	43·65	
	64·98	1·435	1·409	P(023)	65–2491	3·316	10·52	4·389	Orthorhombic	31·92	
	78·11	1·223	1·223	Ni(103)	45–1027	2·6515(4)		4·343(3)	Hexagonal	52·01	
	78·41	1·218	1·219	Ni(220)	88–2326	3·45			Cubic	85·48	
50	38·38	2·344	2·334	P(118)	75–0577	9·21	9·15	22·6	Monoclinic	14·25	48·65
	44·61	2·030	2·03	Ni(111)	01–1260	3·5175			Cubic	43·65	
	64·98	1·435	1·409	P(023)	65–2491	3·316	10·52	4·389	Orthorhombic	47·88	
	78·11	1·223	1·223	Ni(103)	45–1027	2·6515(4)		4·343(3)	Hexagonal	52·01	
	78·40	1·218	1·219	Ni(220)	88–2326	3·45			Cubic	85·47	
90	38·27	2·351	2·334	P(118)	75–0577	9·21	9·15	22·6	Monoclinic	28·5	48·33
	43·55	2·078	2·071	P(131)	76–1965	3·3114(6)	10·189	4·254(1)	Orthorhombic	24·85	
	44·53	2·034	2·034	Ni(111)	65–2865	3·524			Cubic	43·64	
	64·91	1·436	1·409	P(023)	65–2491	3·316	10·52	4·389	Orthorhombic	38·29	
	78·04	1·224	1·223	Ni(103)	45–1027	2·6515(4)		4·343(3)	Hexagonal	69·31	
	78·33	1·219	1·219	Ni(220)	88–2326	3·45			Cubic	85·43	
120	38·23	2·3523	2·3341	P(118)	75–0577	9·21	9·15	22·6	Monoclinic	14·24	36·67
	44·58	2·0324	2·0334	Ni(011)	45–1027	2·6515(4)		4·343(3)	Hexagonal	43·67	
	64·94	1·4358	1·4095	P(023)	65–2491	3·316	10·52	4·389	Orthorhombic	31·91	
	78·08	1·2228	1·2239	Ni(103)	45–1027	2·6515(4)			Hexagonal	56·85	
180	44·53	2·0343	2·0344	Ni(111)	87–0712	3·5238			Hexagonal	5·45	33·54
	65·00	1·4347	1·4095	P(023)	65–2491	3·316	10·52	4·389	Orthorhombic	38·31	
	78·13	1·2218	1·2239	Ni(103)	45–1027	2·6515(4)		4·343(3)	Hexagonal	56·87	
300	44·70	2·0273	2·0297	Ni(111)	70–0989	3·5157			Cubic	58·22	44·27
	65·03	1·4341	1·4095	P(023)	65–2491	3·316	10·52	4·389	Orthorhombic	31·93	
	78·16	1·2218	1·2239	Ni(103)	45–1027	2·6515(4)		4·343(3)	Hexagonal	42·66	
600	44·93	2·0154	2·0344	Ni(111)	01–1266	3·499			Cubic	2·744	48·7
	65·15	1·4305	1·4095	P(023)	65–2491	3·316	10·52	4·389	Orthorhombic	76·81	
	78·28	1·220	1·223	Ni(103)	45–1027	2·6515(4)		4·343(3)	Hexagonal	66·54	
900	65·17	1·430	1·409	P(023)	65–2491	3·316	10·52	4·389	Orthorhombic	42·91	50·64
	78·29	1·220	1·223	Ni(103)	45–1027	2·6515(4)		4·343(3)	Hexagonal	58·36	
1200	65·16	1·430	1·409	P(023)	65–2491	3·316	10·52	4·389	Orthorhombic	39·05	54·79
	78·27	1·220	1·223	Ni(103)	45–1027	2·6515(4)		4·343(3)	Hexagonal	70·52	
1800	65·12	1·431	1·409	P(023)	65–2491	3·316	10·52	4·389	Orthorhombic	69·29	72·28
	78·24	1·220	1·223	Ni(103)	45–1027	2·6515(4)		4·343(3)	Hexagonal	75·27	

By comparing the XRD patterns, it is found that as the deposition time increases, the phosphorus peak occurring at around $2\theta = 38°$ gradually disappears, which indicates that the Ni–P coating occurs on the surface of the anodized aluminium sample with the same plane orientation, P (1 1 8). The sharp peak appearing at around 44° corresponds to the (1 1 1) diffraction of cubic nanocrystalline nickel. On increasing the deposition time (figure 6(f–h)), mixture of amorphous/nanocrystalline peaks is visible up to 600 s. On increasing deposition time, amorphous with nanocrystalline peak is converted into the fully amorphous Ni–P band with low intensity in the range of 40–55° due to the changes in the close packing arrangement of *fcc* Ni. El Mahallawy *et al* (2008) observed that the broad peak might belong to only Ni and P may not be visible because it is amorphous. They noticed that a broad peak with a width larger than 10° occurs as a result of the superposition of Ni and Ni–P alloy peaks at 48–62° which corresponds to an amorphous material. In another study (Sharma *et al* 1998), it was mentioned that the as-deposited coating is amorphous, containing Ni and P separately. Plane orientation changes with time towards more compactness of the deposited Ni–P coatings

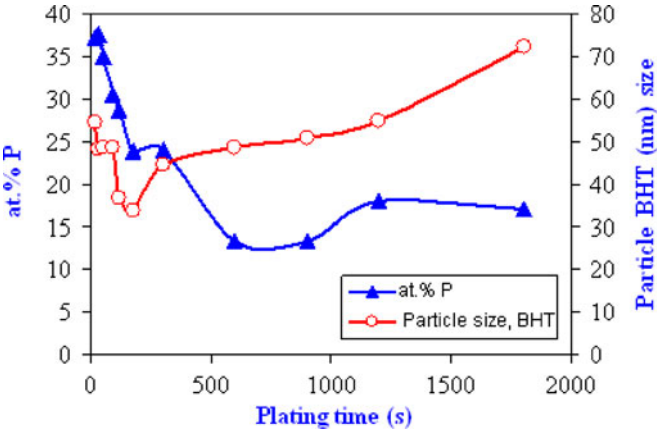

Figure 7. Effect of plating time on atomic percent of phosphorus and particle size.

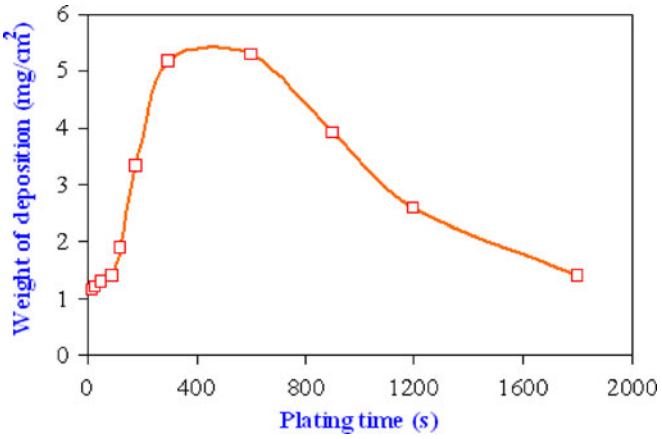

Figure 8. Effect of plating time on weight of deposition.

and the P (0 2 3), Ni (1 0 3) peaks were observed at around 65° and 78° as shown in figure 6(i–k) (Lo *et al* 1994; Zeller and Salvati 1994; Saito *et al* 1999). It confirms that when the deposition time is 1800 s, the coatings have high phosphorous content, which is in good agreement with EDAX analysis.

Figure 7 shows effect of plating time on atomic percentage of phosphorus and particle size of the Ni–P coatings in the as-deposited condition. As the deposition time increases from 20 to 180 s, average crystal size decreases from 54 to 33 nm. After 180 s, crystal size gradually increases. Average crystal size is 72 nm for plating time of 1800 s. However, by increasing deposition time, at.% of phosphorus decreases to some extent and after that, it increases in a parabolic manner. During the initial stages of electroless deposition, both oxidation of reducing agent and reduction of metal ion taking place on a catalytic surface lead to high rate of deposition. Other side reactions are hydrogen evolution and deposition of phosphorus along with nickel. This co-deposition of phosphorous, a non-catalytic material, reduces the rate of deposition continuously. However, P content in the deposit also reduces up to about 180 s and after that, pH of the electrolyte adjacent to the reaction centre reduces slowly due to the formation of H^+ ions. The following reactions favour the deposition of nickel and phosphorus from the hypophosphite bath (Ashassi-Sorkhabi *et al* 2005).

$$Ni^{2+} + 2H_2PO_2^- + 2H_2O \rightarrow Ni + 2H_2PO_3^- + H_2 + 2H^+, \quad (1)$$

$$2H_2PO_2^- + H^+ \rightarrow H_2PO_3^- + P + H + H_2O. \quad (2)$$

Such formation of H^+ favours further P deposition due to the lower pH in the solution than bulk of the electrolyte (Iranipour *et al* 2010; El Mahallawy *et al* 2008). Crystal size variation observed in the plating process, which implies that the crystal growth of the deposited Ni–P is a diffusion controlled process (Guo *et al* 2003).

Figure 8 shows effect of coating time on weight of the Ni–P deposit formed at optimum conditions. As deposition time increases from 20 to 1800 s, weight of the deposit increases up to 600 s and then decreases. Maximum weight of deposit is obtained at the deposition of 600 s. The deposit weight gain curves are nonlinear as reported earlier (Sharma *et al* 1998). Weight of the deposit in the early stage is high due to the presence of a large number of pores in the anodized aluminium and higher specific area. The coating is mainly nanoporous Al_2O_3, which consequently provides more nucleus sites for the nucleation of crystals. This may facilitate the formation of nanocrystalline deposits.

3.5 *UV reflectance study*

Plating time is found to play an important role in the nature and colour of electroless nanocrystalline nickel deposit. As the deposition time increased from 20 to 1800 s, the electroless bath produced brown, dark brown, black, greyish black, grey, light grey with metallic lustre and finally nickel finish on anodized aluminium. This may be due to the gradual filling of nickel deposits in the pores of the anodized aluminium (John *et al* 1983; Srinivasan *et al* 1984; Brown *et al* 2002; Cui *et al* 2006).

UV reflectance of the black to bright nanocrystalline coating on AAO film produced at 20 s is 16·92%, 50 s is 10·76%, 300 s is 11·25%, 600 s is 14·79% and 1200 s is 14·86%. It can be seen that as the deposition time increases, reflectance of the UV light decreases as the black Ni coating absorbs more amount of UV light. Further deposition of nanoparticles of electroless Ni–P at the pores further increases the absorbance of light. About 89% absorption leads to black colour.

4. Conclusions

Electroless nickel deposits on anodic aluminium oxide film formed in 30 s is composed of uniform layer of black Ni–P nanocrystals. Larger number of NC-Ni–P crystals combined to form almost uniform morphology at 1800 s plating time.

Atomic percentage of phosphorus in the Ni–P coating with different plating times follows parabolic manner. As the deposition time increases, reflectance value of NC-Ni–P in the visible region decreases and sharp NC-Ni–P is transformed into amorphous peak indicating crystal growth formation on the surface of the anodized aluminium sample with the same plane orientation.

Acknowledgement

The authors gratefully acknowledge Prof. P Manisankar, Alagappa University, Karaikudi, for his generous help in characterization studies.

References

Apachitei I, Duszczyk J, Katgerman L and Overkamp P J B 1998 *Scr. Mater.* **38** 1347

Ashassi-Sorkhabi H, Mirmohseni A, Harrafi H 2005 *Electrochim. Acta* **50** 5526

Baskaran I, Sankara Narayanan T S N and Stephen A 2006 *Mater. Chem. Phys.* **99** 117

Birks L S and Friedman H 1946 *J. Appl. Phys.* **17** 687

Brenner A and Riddell G E 1946 *J. Res. Nat. Bur. Stand.* **37** 31

Brown R J C, Brewer P J and Milton M J T 2002 *J. Mater. Chem.* **12** 2749

Chow G M and Ovid'ko I 2000 *Nano-structured films and coatings*, North Atlantic Treaty Organization (NATO) Science Series, 3. High Technology (ed.) T Tsakalakos (Dordrecht: Kluwer Academic Publishers) **vol. 78**

Cui G, Li N, Li D, Zheng J and Wu Q 2006 *Surf. Coat. Technol.* **200** 6808

El Mahallawy N, Bakkar A, Shoeib M, Palkowski H and Neubert V 2008 *Surf. Coat. Technol.* **202** 5151

Fundo A M and Abrantes L M 2007 *J. Electroanal. Chem.* **600** 63

Goldenstein A W, Rostoker W, Schossberger F and Gutzeit G 1957 *J. Electrochem. Soc.* **104** 104

Goueffon Y, Arurault L, Mabru C, Tonon C and Guigue P 2009 *J. Mater. Process. Technol.* **209** 5145

Guo Z, Keong K G and Sha W 2003 *J. Alloys Compd.* **358** 112

Huang Y S and Cui F Z 2007 *Surf. Coat. Technol.* **201** 5416

Hur K H, Jeong J H and Lee D N 1990 *J. Mater. Sci.* **25** 2573

Iranipour N, Azari Khosroshahi R and Parvini Ahmadi N 2010 *Surf. Coat. Technol.* **205** 2281

John S, Shanmugan N V, Srinivasan K N, Selvam M and Shenoi B A 1983 *Surf. Coat. Technol.* **20** 331

Keong K G, Sha W and Malinov S 2002 *J. Alloys Compd.* **334** 192

Kumar P S and Nair P K 1994 *J. Mater. Sci. Lett.* **13** 671

Li L B, An M Z and Wu G H 2005 *Mater. Chem. Phys.* **94** 159

Liu Z and Gao W 2006 *Surf. Coat. Technol.* **200** 3553

Lo P H, Tsai W T, Lee J T and Hung M P 1994 *Surf. Coat. Technol.* **67** 27

Lu G and Zangari G 2002 *Electrochim. Acta* **47** 2969

Mallory G O and Hajdu J B 1990 *Electroless plating* (Norwich, New York: American Electroplaters and Surface Finishing Society)

Martyak N M and Drake K 2000 *J. Alloys Compd.* **312** 30

Masuda H and Fukuda K 1995 *Science* **268** 1466

Meyer M A, Mishra A and Benson D 2006 *J. Prog. Mater. Sci.* **51** 427

Parker K 1992 *Plat. Surf. Finish.* **79** 31

Saito T, Sato E, Matsuoka M and Iwakura C 1999 *Plat. Surf. Finish.* **2** 23

Sevugan K, Selvam M, Srinivasan K N, Vasudevan T and Manisankar P 1993 *Plat. Surf. Finish.* **80** 56

Shacham-Diamad Y and Sverdlov Y 2000 *Microelectron. Eng.* **50** 525

Sharma A K, Suresh M R, Bhojraj H, Narayanamurthy H and Sahu S P 1998 *Met. Finish.* **3** 10

Srinivasan K N, Shanmugan N V, Selvam M, John S and Shenoi B A 1984 *Energy Convers. Manage.* **24** 255

Tyagi S V S, Tandon V K and Ray S 1985 *Metallkde Z.* **76** 492

Wang X C, Cai W B, Wang W J, Liu H T and Yu Z Z 2003 *Surf. Coat. Technol.* **168** 300

Yajima S, Matsashita S, Togawa Y and Kanbe T 1987 *Met. Finish.* **1** 53

Zeller R L and Salvati L 1994 *Corros. Sci.* **6** 457

Zhao H, Huang Z and Cui J 2007 *Surf. Coat. Technol.* **202** 133